

# Time-resolved Studies for the Mechanism of Reduction of Copper Oxides with Carbon Monoxide: Complex Behavior of Lattice Oxygen and the Formation of Suboxides

Xianqin Wang,<sup>†</sup> Jonathan C. Hanson,<sup>†</sup> Anatoly I. Frenkel,<sup>‡</sup> Jaw-Yong Kim,<sup>†,§</sup> and José A. Rodriguez<sup>\*,†</sup>

Chemistry Department, Brookhaven National Laboratory, Upton, New York, 11973, Physics Department, Yeshiva University, New York, New York 10016, and Beamline Division, Pohang Accelerator Laboratory, Pohang, 790–784, South Korea

Received: May 20, 2004; In Final Form: June 22, 2004

Temperature-programmed reduction (TPR), synchrotron-based time-resolved X-ray diffraction (TR-XRD), extended X-ray absorption fine-structure (EXAFS), and X-ray absorption near-edge structure (XANES) were employed in this work to systematically study the reaction of CuO and Cu<sub>2</sub>O with CO gas molecules. Both TPR and isothermal reduction results showed that CuO was easier to reduce than Cu<sub>2</sub>O under the same reaction conditions. In situ measurements of XRD and XANES showed a direct transformation pathway for CuO reduction (CuO → Cu) when there was a large supply of CO, while they showed a sequential step pathway involving one intermediate (CuO → Cu<sub>2</sub>O → Cu) with a limited supply of CO. An induction period for CuO reduction was seen and increased with decreasing temperature. O vacancies in CuO were observed during the induction period that could foster formation of a nonstoichiometric metastable copper-oxide species. The metastable species can either react rapidly with CO to form metallic copper during high CO flow rates or can relax into a Cu<sub>2</sub>O lattice when the supply of CO is limited. The Cu<sub>2</sub>O-like intermediate showed extra disordered oxygen in the empty tetrahedral sites of Cu<sub>2</sub>O. Based on these observations, a possible mechanism for CuO reduction is proposed. This study demonstrates that the mechanism for the reduction of an oxide by CO can vary considerably with the experimental conditions (gas flow rate, temperature, sample size, etc.), and its complex kinetics cannot be described by a single n<sup>th</sup>-order expression over the entire range of reaction. The behavior of CuO-based catalysts is discussed in the light of these results.

## 1. Introduction

CO oxidation is of prime importance to fundamental studies in catalysis, pollution control, and feed purification for fuel cell applications. To meet increasingly stringent environmental regulations in exhaust emission control, the complete oxidation of carbon monoxide is crucial.<sup>1</sup> Precious metals (Pd, Pt, Rh) have traditionally been used as the most efficient catalysts with high activity and stability for this process. However, owing to the high cost and lack of availability of the precious metals, considerable attention has been paid to transition metals and their oxides.<sup>1,2</sup> Among these systems, CuO<sub>x</sub> is one of the most widely used catalysts because of its high activity and selectivity as an oxidation/reduction catalyst. Furthermore, for many years CuO-based catalysts have also been used for reactions that involve the conversion of CO, such as alcohol synthesis (CO + 2H<sub>2</sub> → CH<sub>3</sub>OH)<sup>3</sup> and the water-gas shift reaction (CO + H<sub>2</sub>O → CO<sub>2</sub> + H<sub>2</sub>).<sup>4</sup> CuO, Cu<sub>4</sub>O<sub>3</sub> and Cu<sub>2</sub>O are well-known copper oxides with monoclinic, tetragonal, and cubic crystal structures, respectively (Figure 1).<sup>5–8</sup> Thermodynamically, the oxidation state of copper changes among CuO, Cu<sub>2</sub>O, and Cu as a function of temperature and oxygen partial pressure.<sup>9,10</sup> Three possible pathways for the transformation of CuO to Cu are displayed in Figure 1, including direct reduction (CuO → Cu, pathway 1) and reduction mechanisms that involve either

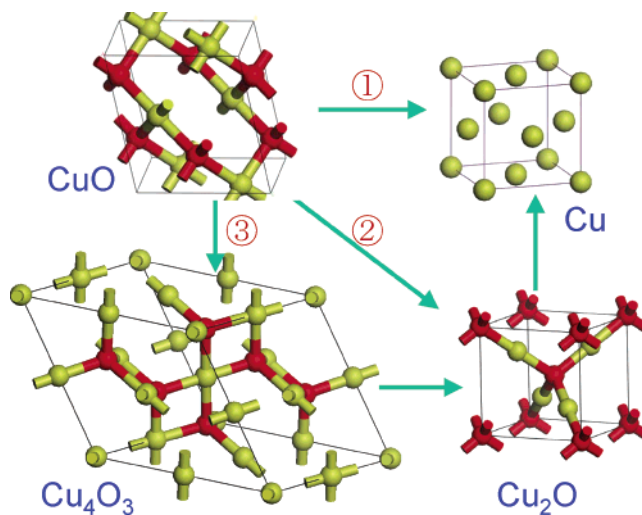


**Figure 1.** Possible pathways for the reduction of CuO to Cu. Notice the significant differences in the crystal structures of CuO, Cu<sub>4</sub>O<sub>3</sub>, and Cu<sub>2</sub>O. In Cu<sub>4</sub>O<sub>3</sub>, half of the Cu atoms have four O neighbors, while the other half of the Cu atoms have only two O neighbors.

one intermediate (CuO → Cu<sub>2</sub>O → Cu, pathway 2) or two intermediates (CuO → Cu<sub>4</sub>O<sub>3</sub> → Cu<sub>2</sub>O → Cu, pathway 3). The main objective of this work is to identify the routes for CuO reduction with CO under different experimental conditions.

Despite the tremendous amount of work carried out to explore the active sites and mechanism for the transformation of CO over all kinds of copper-oxide-based catalysts (CuO/ZnO, CuO/

\* Corresponding author, fax: 631-344-5815, e-mail: rodriguez@bnl.gov.

<sup>†</sup> Brookhaven National Laboratory.

<sup>‡</sup> Yeshiva University.

<sup>§</sup> Pohang Accelerator Laboratory.

CeO<sub>2</sub>, CuO/ZrCeO<sub>4</sub>, CuAl<sub>2</sub>O<sub>4</sub>, and CuCr<sub>2</sub>O<sub>4</sub> spinels, etc.),<sup>11–17</sup> the behavior of copper oxides in the presence of CO still needs to be investigated. For example, during the synthesis of alcohols from CO and the water-gas shift reaction, CuO undergoes partial or total reduction, and for years there has been a controversy about the relative activity of “Cu<sup>+</sup>” and “Cu<sup>0</sup>” centers.<sup>18–20</sup> In the case of CO oxidation, it is believed that defects and oxygen holes could be the reason for the high activity or selectivity of copper-oxide catalysts.<sup>17</sup> Nonstoichiometric metastable copper oxide species formed during reduction or reaction could also play a key role in CO oxidation,<sup>21</sup> but it is not well established how to generate them and control their concentration. This is not a trivial task and requires the use of techniques that allow in situ characterization under reaction conditions.

To the best of our knowledge, no systematic studies have been reported examining in situ the interaction of CO with pure copper oxides (Cu<sub>y</sub>O,  $y = 1$  or  $2$ ), and the concurring reactions of CO oxidation and Cu<sub>y</sub>O reduction. In general, very little is known about the microscopic phenomena associated with the reduction of metal oxides by CO.<sup>22</sup> In principle, this complex process could be controlled by one or multiple reaction steps: creation of sites for the adsorption of CO, formation of CO<sub>2</sub> and removal of oxygen, migration of oxygen from the bulk to the surface, formation of suboxides, phase transformations, growth or nucleation of the reduced metal, etc. Recently, copper oxide reduction by H<sub>2</sub> gas was studied in situ using time-resolved X-ray diffraction.<sup>23,24</sup> This powerful technique is the result of combining the high intensity of synchrotron radiation with rapid new parallel data-collection devices.<sup>25</sup> Time-resolved X-ray diffraction (XRD) was used in the present work to monitor chemical transformations and the long-range atomic order of CuO and Cu<sub>2</sub>O during CO oxidation. Information about the short-range atomic order and local geometry of Cu was obtained by collecting data of time-resolved X-ray absorption fine structure (XAFS), which was analyzed using the principal component analysis (PCA) method.<sup>26</sup>

## 2. Experimental Section

**2.1 Temperature-programmed Reduction (TPR).** In addition to carrying out the reaction between CO and copper oxide powders at isothermal conditions, each copper oxide was reduced to Cu by temperature-programmed reduction with a linear heating rate under sufficient and insufficient gas supply conditions.

The CuO and Cu<sub>2</sub>O powders were obtained from commercial sources (>99.99% purity). For the normal reduction conditions (i.e., typical flow of CO gas, standard packing of the oxide in a flow reactor), a fresh sample (5 mg) was loaded in a clean sapphire reactor tube<sup>27</sup> with an 0.5-mm i.d. before each run. Quartzwool was added on each side of the powder to keep the sample position constant during the gas flowing. A small resistance heater was placed below the sapphire capillary that contained the sample. A thermocouple (Type K) was inserted into the capillary near the powder to measure the temperature throughout the measurements and to provide input for the temperature controller.<sup>27</sup> The catalyst sample was reduced by flowing a 5% CO (99.9999% purity) and 95% He (99.9999% purity) gas mixture (15–20 mL/min) and heating from 25 to 725 °C in 2 h. For the abnormal reduction conditions, the fine CuO and Cu<sub>2</sub>O powders were uniformly spread with a brush over adhesive Kapton polyamide tape. A strip of the tape was loaded into a Kapton tube. Kapton is relatively transparent for X-rays at the 9–10 keV energy range, does not decompose at temperatures up to 400 °C, and thus makes a good support.

Except for the much slower flow rate (1–5 mL/min), the rest of the experimental setup for the tape-loaded sample was the same as the one used for normal-condition operation.

TPR experiments were carried out using the fixed-bed sapphire microreactor<sup>27</sup> described above, which was connected to a 0–100 amu quadrupole mass spectrometer (QMS, Stanford Research Systems). A portion of the exit gas flow passed through a leak valve and into the QMS vacuum chamber. QMS signals at mass-to-charge ratios of 4(He), 18(H<sub>2</sub>O), 28(CO), 32(O<sub>2</sub>), 44(CO<sub>2</sub>), and 12(C) were monitored during the experiments, and these and the temperature increase were recorded at the same time by an online computer. Phase changes of the sample were identified with time-resolved XRD data collected at the *same* time as the reduction experiments.

**2.2 Time-resolved XRD and Data Processing.** The time-resolved X-ray diffraction data were collected at the beamline  $\times 7B$  ( $\lambda = 0.9225$  Å) of the National Synchrotron Light Source (NSLS) in Brookhaven National Laboratory (BNL) using a MAR345 area detector. An identical setup system as that in the TPR experiments was employed for the XRD experiments under both normal and abnormal conditions. Besides time-resolved XRD patterns collected during TPR experiments, the XRD patterns were also recorded during isothermal runs at different temperatures under small or larger CO flow conditions over Kapton-taped samples. The temperatures were calibrated with a linear curve of the Cu cell expansion as a function of temperature.<sup>28</sup> The original powder rings were integrated with the FIT2D code.<sup>29</sup> The FIT2D parameters for the integration of the data were obtained with a standard LaB<sub>6</sub> crystal compound. A two-dimensional (2D) chart document was obtained with a Fortran CHITOUXDS code, and the time-resolved XRD pattern files were plotted with an IDL code.<sup>30</sup> The powder profiles from the isothermal data at 224 °C were analyzed using the GSAS program.<sup>31</sup> In addition to the usual powder profile and scale parameters, the weight fraction of each phase and selected oxygen occupancies were refined. The ordered oxygen parameters were refined for copper oxides, and an “extra” oxygen that fits in the unoccupied tetrahedral space in Cu<sub>2</sub>O was refined.

**2.3 Time-resolved X-ray Absorption Spectroscopy and Data Processing.** The time-resolved X-ray absorption spectroscopy (XAS) measurements were performed in beamline  $\times 16C$  of the NSLS at BNL using a setup similar to that of our previous time-resolved studies.<sup>24</sup> First, the sample was brushed onto an adhesive Kapton tape. Next, the strip of Kapton tape was loaded into the same cell used for in situ XRD and heated to the desired temperature. It was then exposed to a flow of a 5% CO and 95% He gas mixture ( $\sim 1$  mL/min) while the X-ray absorption spectra were taken repeatedly during reaction. The isothermal reductions were repeated at several temperatures, the lowest being 300 °C. The absorption edge steps, measured in transmission mode, on all the samples were ca. 0.2–0.25 at the Cu K absorption edge (8978 eV). EXAFS scans from 150 eV below the Cu K-edge to 800 eV above were measured for the samples reduced at the lowest temperature (300 °C) for which the duration of reaction was more than an hour; each EXAFS scan lasted 10 min. At relatively high temperatures (above  $\sim 350$  °C) that made EXAFS data collection impractical due to the short (tens of minutes) reaction times, XANES measurements were taken instead; each XANES scan took about 4 min. The start of the first scan at each temperature was synchronized with the beginning of the CO flow, and the data were taken until the difference between the successive spectra became smaller than the statistical noise in the data. After reduction, the full EXAFS measurement was taken again after

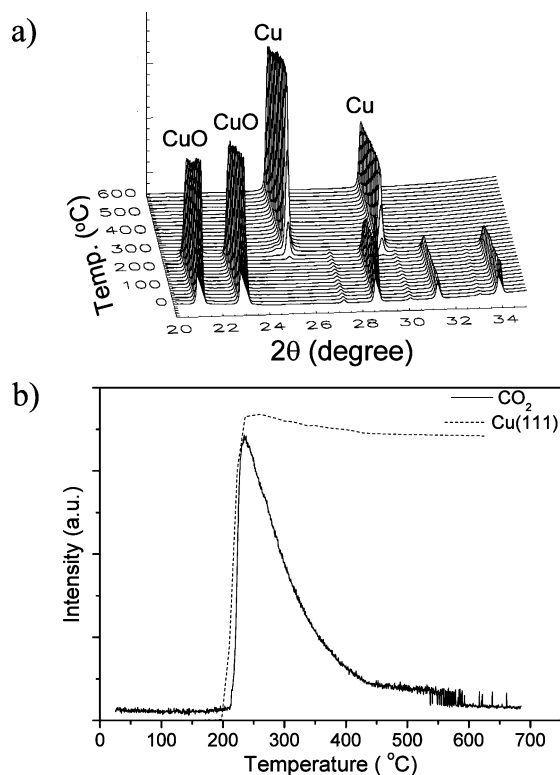


**Figure 2.** Temperature-programmed reduction of CuO. (Temperature increase rate ( $\beta$ ) = 350 °C/h or 5.8 °C/min; 5% CO/95% He gas flow rate  $\approx$  15–20 mL/min). Panel a: TR-XRD patterns; Panel b: Intensities for the Cu (111) diffraction line in XRD and the  $\text{CO}_2$  signal ( $m/z = 44$  in QMS) at the exit of the reactor.

the sample was cooled to room temperature, to determine how much pure Cu was in the sample by comparing with the spectrum from the Cu foil that was measured simultaneously in reference mode. The sample temperatures during these XAFS experiments were accurately calibrated by comparing the best-fit results for the first nearest neighbor (Cu–Cu) EXAFS Debye–Waller factor ( $\sigma^2$ ) obtained for the fully reduced Cu sample at each temperature and their theoretical values calculated by using the correlated Einstein model.<sup>32</sup> This procedure can be implemented by using the software program FEFFFIT.<sup>33</sup>

### 3. Results

**3.1 Temperature-programmed Reduction.** Figure 2 shows typical results for the temperature-programmed reduction of CuO with carbon monoxide. The time-resolved XRD patterns in Figure 2a indicate that CuO started to reduce to metallic Cu at a temperature of  $\sim 200$  °C, and was completely transformed to Cu at 236 °C. No intermediate phase was seen during the reduction process. CO was oxidized to  $\text{CO}_2$ , and the QMS trace of  $\text{CO}_2$  and the intensity change for the peak Cu(111) line in XRD are plotted as a function of temperature in Figure 2b. The setout point for the  $\text{CO}_2$  signal was  $\sim 210$  °C; it rapidly reached its maximum at 236 °C, and then tailed off gradually until the temperature reached 585 °C. The results indicate that part of the  $\text{CO}_2$  product may have chemisorbed on the walls of the detection system and gradually desorbed (a common problem in CO-TPR experiments). The  $\text{CO}_2$  peak temperature observed in this work was close to those reported for supported copper oxide catalysts.<sup>34</sup> Time-resolved XRD patterns for  $\text{Cu}_2\text{O}$  reduction showed similar trends to those for CuO reduction with a direct transformation to metallic Cu; the results are not shown here.

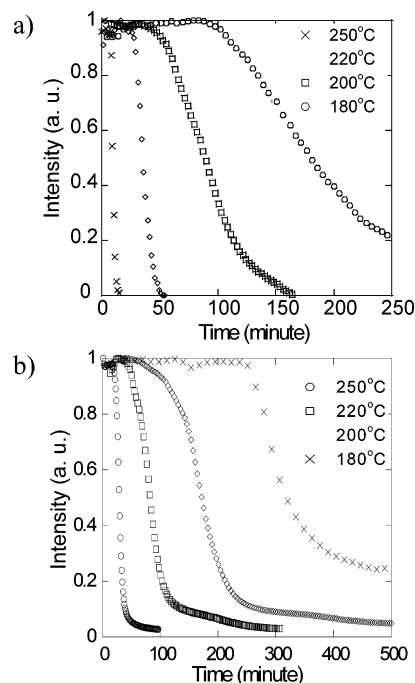


**Figure 3.** Isothermal reductions carried out in a sapphire tube at different temperatures (gas flow rate  $\approx$  15–20 mL/min). (a) CuO (111) intensity as a function of time in isothermal reduction experiments of CuO; (b)  $\text{Cu}_2\text{O}$  (111) intensity as a function of time in isothermal reduction experiments of  $\text{Cu}_2\text{O}$ .

**3.2 Isothermal Reduction XRD Results.** The use of linear heating rates in TPR results in nonuniform reaction conditions throughout the sample leading to relatively poor resolution in the kinetic data. Thus, isothermal reduction experiments were also carried out with the packed samples at temperatures of 180, 200, 220, and 250 °C under a large supply of CO (5% CO/95% He gas mixture with a flow rate of 15–20  $\text{cm}^3/\text{min}$ ).

The normalized CuO (111) and  $\text{Cu}_2\text{O}$  (111) peak intensities as a function of time for the reductions of CuO and  $\text{Cu}_2\text{O}$  are shown in Figures 3a and 3b, respectively. The time-resolved X-ray diffraction patterns were similar to those obtained by TPR methods with no intermediate phases and are not shown here. *The isothermal reduction experiments revealed the existence of an induction period.* This induction period became shorter with increasing temperature. For instance, the induction periods were around 100 min, 50 min, and 25 min for the reaction temperatures of 180 °C, 200 °C, and 220 °C, respectively (Figure 3a). The reaction was faster at higher operating temperatures. Figure 3b represents the change for the intensity of the  $\text{Cu}_2\text{O}$  phase during the isothermal reduction as a function of time. Similarly, *an induction period was also observed for each experiment*, and the effect of temperature on the induction period and the reaction rate followed the same trends as those for CuO reduction (Figure 3a). However, the induction time for  $\text{Cu}_2\text{O}$  reduction was longer than that for CuO reduction at the same temperature. Moreover, unlike CuO reduction (which could be completed during a reasonable time), a small amount of  $\text{Cu}_2\text{O}$  was always observed in the compounds at the end of each experiment, though the amount in the system decreased with the increase of the operating temperature. *These results indicate that  $\text{Cu}_2\text{O}$  was harder to be reduced than CuO under the same operating conditions.*

Isothermal reductions of CuO powder on Kapton tape were also carried out at several temperatures with a *very low* supply of CO (5% CO/95% He gas mixture with a flow rate of  $\sim 1$  mL/min). Typical time-resolved XRD patterns for this kind of

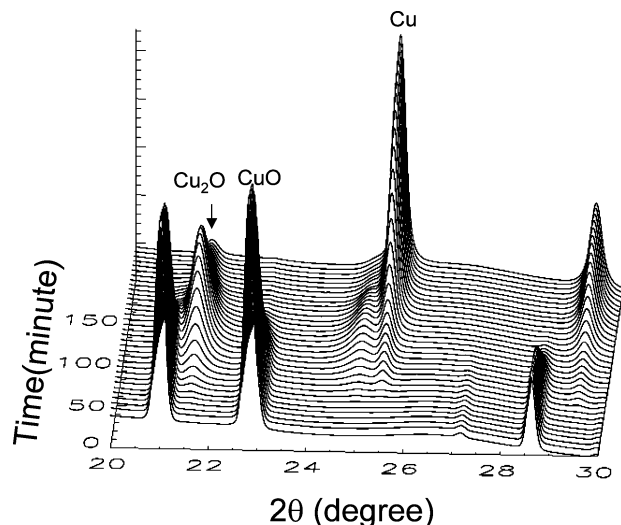


**Figure 4.** TR-XRD patterns for the isothermal reduction of CuO spread evenly on a Kapton tape (Temperature: 224 °C; 5% CO/95% He gas flow rate  $\approx$  1 mL/min).

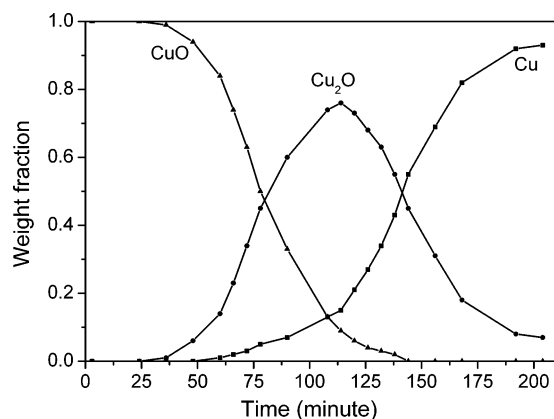
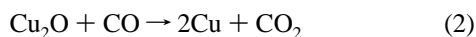


**Figure 5.** Weight fractions of CuO, Cu<sub>2</sub>O, and Cu as a function of time for the XRD data in Figure 4. The results were obtained with the GSAS program.

experiment are shown in Figure 4, which displays reduction data at 224 °C. Unlike the results shown earlier (Figures 2–3), a Cu<sub>2</sub>O phase was clearly observed in these experiments. The phases CuO, Cu<sub>2</sub>O, and Cu were fitted to the patterns and the profiles refined with the GSAS program. Figure 5 shows the weight fractions of Cu<sub>x</sub>O species as a function of time. The results indicated that, *under a limited supply of CO*, CuO started to transform to Cu<sub>2</sub>O after an induction period of 35 min, and the whole reduction process followed a sequential step reduction mechanism



that essentially involves the reverse steps for the mechanism of Cu oxidation with O<sub>2</sub>.<sup>24</sup> The formed intermediate phase, Cu<sub>2</sub>O, could not be completely transformed to metallic copper, as was observed in Figure 3b. It is also important to notice that, even with a limited supply of CO, we never detected Cu<sub>4</sub>O<sub>3</sub> as an intermediate or suboxide in the reduction of CuO.

**3.3 XAFS Results.** Time-resolved XANES/EXAFS experiments were carried out for the reduction of copper oxide at different temperatures to independently verify the step reduction mechanism and check for a possible amorphous CuO<sub>x</sub> phase as an intermediate not detected with XRD.

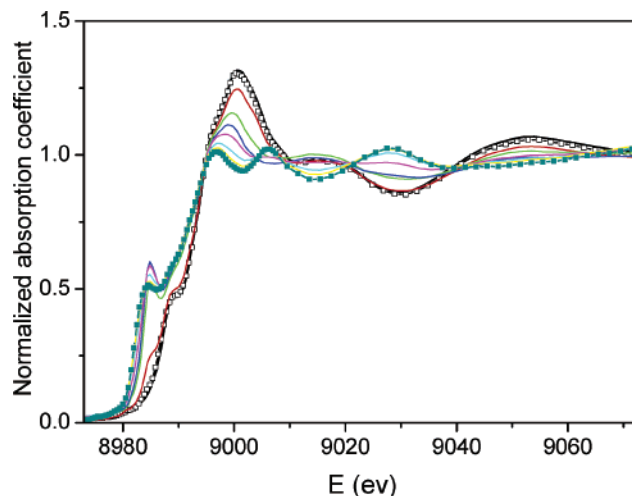


**Figure 6.** Plot of time-resolved XANES for the isothermal reduction of CuO at 300 °C. (CuO spread evenly on a Kapton tape; 5% CO/95% He gas flow rate  $\approx$  1 mL/min).

In agreement with the XRD results, the XANES and EXAFS results indicated the step reduction of CuO for all the temperatures studied here under a limited supply of CO. Figure 6 presents typical XANES spectra taken at 300 °C. The spectra obtained at other temperatures showed a similar trend, and are not shown here. The starting spectrum from CuO gradually transformed into the corresponding spectrum for Cu. The fact that the sample's reduction to pure Cu was virtually 100% was confirmed by comparing the XAS spectra in reference metal Cu foil with the product of the reaction taken after cooling the sample down to room temperature. The small discrepancy in amplitude is attributed to the extra disorder in the freshly reduced sample. The changes in the near-edge region that occurred during the reduction are apparent. *The absence of an isosbestic point in the XANES spectra indicates the presence of more than two species during the reaction.* For comparison, in our previous time-resolved XAS studies, we did observe isosbestic points in those spectra for which the PCA showed conclusively no presence of an intermediate phase at any time during the reductions.<sup>23–24,35</sup>

Figures 7a and 7b show the  $k^2$ -weighted EXAFS and Fourier transform magnitudes (uncorrected for photoelectron phase shifts), respectively, of the X-ray absorption coefficient data collected during CuO reduction at 300 °C. The data are clearly sensitive to the changes in the Cu coordination during the reduction. The data demonstrate a gradual decrease in the intensity of the lower  $r$  peak corresponding to the Cu–O bond in CuO (Figure 7b). This decrease was accompanied by the gradual rise of the higher  $r$  peak corresponding to the Cu–Cu first-nearest-neighbor distance in metallic Cu. However, based on visual observation only, the presence of an intermediate Cu<sub>2</sub>O and/or other Cu<sub>x</sub>O phases in CuO reduction could neither be confirmed nor ruled out.

PCA is not a model-dependent XAFS data analysis method because (1) the number  $N$  of principal components is found model-independently, and (2) the identity of individual species composing the sample is obtained by a *linear* combination of  $N$  principal components, and the “wrong” standards can often be ruled out based on the quality of the fits.<sup>23,24</sup> If a more traditional (fitting) EXAFS data analysis approach were used, their separate structural analysis would be strongly model-dependent and less reliable. After applying the PCA to the series of XANES and EXAFS spectra taken at different temperatures, the PCA scree tests demonstrated convincingly that three

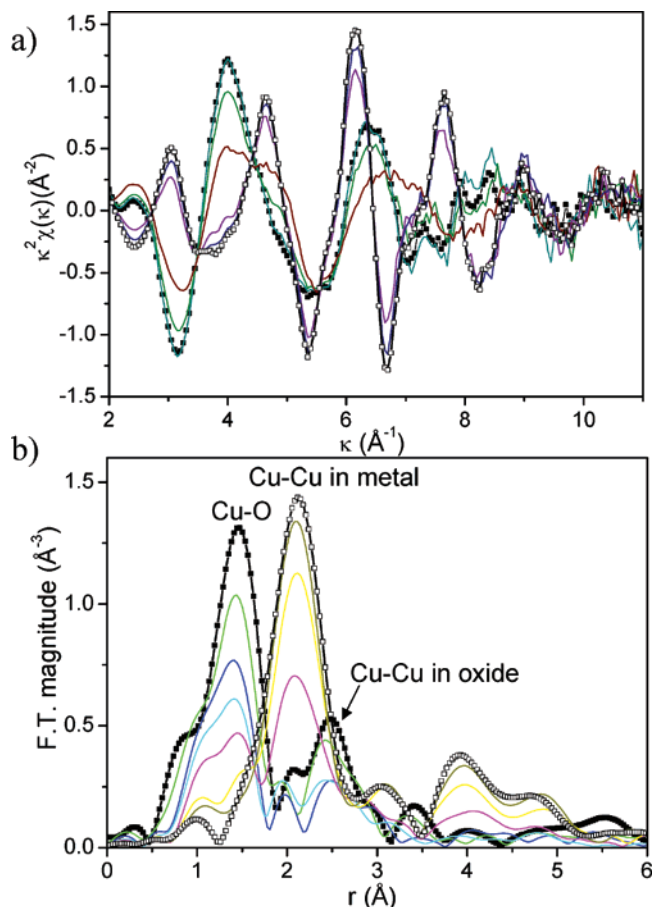


**Figure 7.** Time-resolved EXAFS spectra in (a)  $k$ -space and (b)  $r$ -space for the isothermal reduction of CuO at 300 °C. (CuO spread evenly on a Kapton tape; 5% CO/95% He gas flow rate  $\approx$  1 mL/min). The filled squares correspond to the initial oxides, whereas the open ones denote the final product.

components (phases) were needed to adequately fit the spectra (Figure 8a). Therefore, it could be expected that at least three phases were present during the CuO reduction. It is most reasonable to expect that these phases are the starting phase (CuO), the resultant phase (Cu), and the intermediate phase (Cu<sub>2</sub>O); however, this hypothesis must be confirmed by the quantitative analysis. The three components obtained from the PCA analysis of raw XANES (or EXAFS) spectra were first fitted to standard compounds (e.g., metal copper and copper oxides as the most probable species to be found in the data). When a good fit to each standard is obtained, it points to the presence of that respective species in the sample. After all species are identified by fitting the principal components to the standard spectra, these spectra are then combined to simulate the EXAFS or XANES spectra at each time step, the mixing fractions of these species being the only variables that differ one time step datum from another. These mixing fractions are then varied to best fit the experimental data collected during reaction at all times. In our case, the different linear combinations of the same three principal components were fitted perfectly to (a) pure CuO, (b) pure Cu<sub>2</sub>O, and (c) pure Cu data measured at the same temperatures, by only varying the weighting factors of the components. This procedure was performed for data taken at all temperatures. An example of the fitting result from the data at 300 °C is shown in Figure 8b. The figure presents the molecular fractions of three different species as a function of time. *It is evident that the step reduction CuO  $\rightarrow$  Cu<sub>2</sub>O  $\rightarrow$  Cu was confirmed with the XAFS technique.*

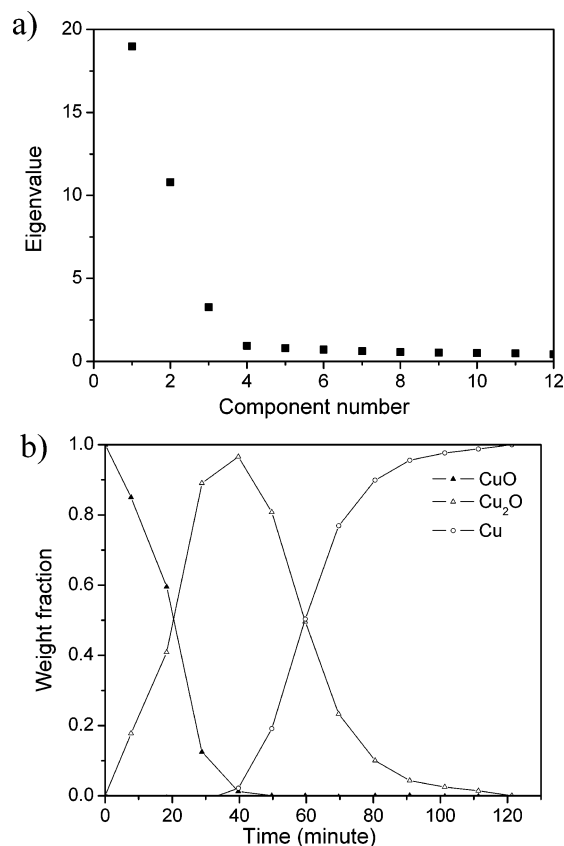


**Figure 8.** (a) PCA scree test for the EXAFS data in Figure 7A. (b) CuO, Cu<sub>2</sub>O, and Cu weight fractions during the time-resolved XANES spectra of the isothermal reduction at 300 °C obtained from PCA. (CuO spread evenly on a Kapton tape; 5% CO/95% He gas flow rate  $\approx$  1 mL/min).

Furthermore, neither Cu<sub>4</sub>O<sub>3</sub> nor an amorphous CuO<sub>x</sub> phase was formed during the reduction of CuO by CO. Compared to the XRD results obtained with the same setup (Figure 4), no induction time and complete reduction of CuO were seen, probably because a higher temperature (300 °C) was employed here.

#### 4. Discussion

In this work, two pathways for the CuO  $\rightarrow$  Cu reaction were observed under different operating conditions. A direct transformation (pathway 1 in Figure 1) was seen for samples under a high CO/He gas flow rate (Figures 2a, 3a), while a reduction mechanism with one intermediate (pathway 2 in Figure 1) was obtained for samples under a low CO/He gas flow rate (Figures 5, 8). Pathway 3 in Figure 1 requires the observation of Cu<sub>4</sub>O<sub>3</sub> as an intermediate, but this species was not seen in this work (Figures 2a, 3a). This is somewhat surprising, because Cu<sub>4</sub>O<sub>3</sub> is much more stable than a CuO with 25% oxygen vacancies in DFT calculations.<sup>23</sup> Furthermore, Cu<sub>4</sub>O<sub>3</sub> appears as a logical intermediate between CuO and Cu<sub>2</sub>O, with half of the Cu atoms in a “+2” formal oxidation state and the other half in a “+1” formal oxidation state.<sup>23</sup> The absence of pathway 3 can be rationalized in kinetic terms because it requires a precise rearrangement of O atoms as shown in Figure 9. The formation of Cu<sub>4</sub>O<sub>3</sub> needs the specific removal of the oxygen colored yellow in the figure from CuO without elimination of the oxygen colored blue in the figure. However, during reduction, part of the blue-colored oxygen could be removed faster than the yellow-colored oxygen, making the formation of Cu<sub>4</sub>O<sub>3</sub> very difficult before Cu<sub>2</sub>O is seen.

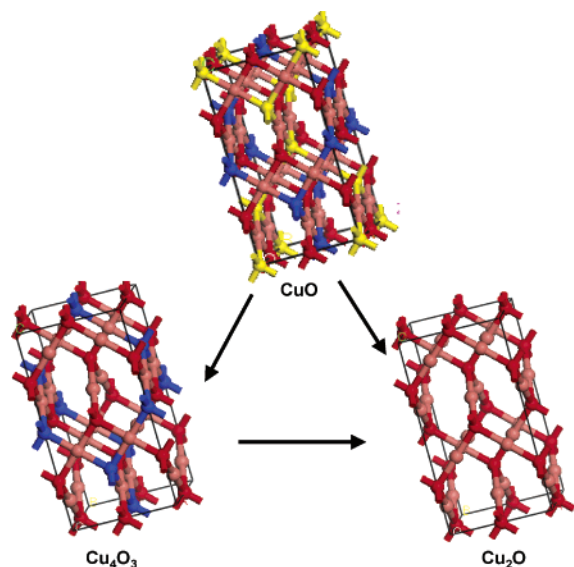


**Figure 9.** Oxygen removal from a hypothetical tetragonal CuO in a common space group  $I_1/amd$  to form  $Cu_4O_3$  (removal of oxygen in yellow) and  $Cu_2O$  (removal of oxygen in both yellow and blue).

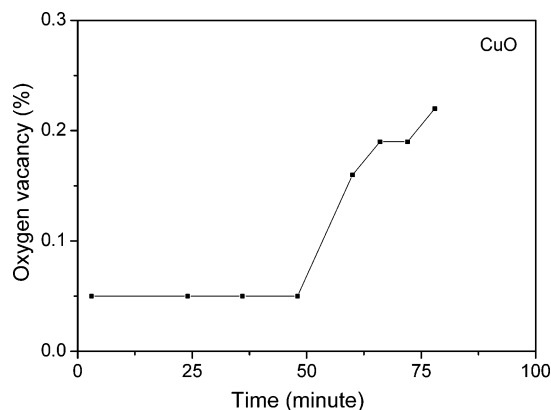


**Figure 10.** Oxygen vacancies in CuO as a function of time for the XRD results in Figure 4. The O occupancies were obtained with the GSAS program.

Evidence for O vacancies in CuO during reduction is observed from the profile refinement of the XRD results in Figure 4 (see Figure 10). The maximum amount of O vacancies found is less than 25%. The O vacancies in CuO could foster formation of a nonstoichiometric metastable copper-oxide species.<sup>16,23</sup> This metastable species can either react rapidly with CO to form metallic copper under high CO flow rates (pathway 1 in Figure 1) or relax into  $Cu_2O$  when the supply of CO is limited (pathway 2 in Figure 1). At slow flow rates of CO, the O atoms have more time for rearrangement, so a pathway to form the thermodynamically stable  $Cu_2O$  can occur.

In the X-ray structure refinements and difference electron density maps, two different kinds of extra electron densities were observed in addition to the densities from the lattice Cu (0 0 0) and oxygen (0.25 0.25 0.25) in the  $Cu_2O$  phase formed during the reduction process. The less intense one at the middle of the Cu–Cu chain (Cu–Cu distance 3.02 Å) has been reported to be the electron densities from Cu–Cu covalent bonding.<sup>36</sup> The intense one partially filling the positions for the yellow and blue O atoms in Figure 9 is tentatively assigned to extra oxygen atoms in a  $Cu_2O$  lattice. The lattice of  $Cu_2O$  (77.4 Å<sup>3</sup>) has a similar volume to that of CuO (81.5 Å<sup>3</sup>), therefore,  $Cu_2O$  could embrace extra O atoms. These extra oxygens must be disordered and have fractional occupancy less than 0.33 that would result

**TABLE 1**

	extra oxygen <sup>a</sup> occupancy in $Cu_2O$	wt. % $Cu_2O$
pure $Cu_2O$	~0.00 (2)	00
$CuO$ reduction intermediate ( $Cu_2O$ )	0.17 (1) <sup>b</sup>	74

<sup>a</sup> Extra oxygen position at (0.25 0.75 0.25) with multiplicity of 6, while the normal lattice oxygen is at (0.25 0.25 0.25). <sup>b</sup> Occupancy was refined when there was 74%  $Cu_2O$  intermediate phase in the system.

in stoichiometric CuO. Structures can be chosen that would have the connectivity patterns in CuO and  $Cu_4O_3$  (see Figure 9). These structures must be highly strained because the observed  $Cu_2O$  lattice requires that all distances be 1.85 Å, which is the  $Cu^{1+}$ –O distance. However, if there is extra oxygen in the lattice, some of the copper must be in the +2 oxidation state, which has the longer Cu–O distance, approaching 1.95 Å. The structural changes from CuO to  $Cu_2O$  could be described as successively distorting the observed monoclinic structure to a hypothetical tetragonal CuO arrangement and then removing bridging oxygen atoms between the copper atoms until the cubic  $Cu_2O$  structure is formed. The latter structures can be drawn in a common space group  $I_1/amd$  (Figure 9).<sup>7</sup> The observation of “extra” oxygen in the  $Cu_2O$  phase can be rationalized in terms of the requirement of this structure to rearrange from the more random orientation in CuO. The extra oxygen occupancy in the intermediate  $Cu_2O$  is compared to that obtained from the pure  $Cu_2O$  in Table 1. These results clearly imply that the intermediate  $Cu_2O$  phase formed during CuO reduction had an observable amount of extra oxygen. However, because of the limitations of XRD techniques for the detection of light elements, the presence of the extra oxygen atoms needs to be confirmed in the future with other techniques, such as neutron diffraction.

Unlike CuO reduction,  $Cu_2O$  reduction has only one apparent pathway involving two phases ( $Cu_2O \rightarrow Cu$ ), but amorphous suboxides could be formed. The presence of the latter can be ruled out based on our XANES/EXAFS results. It was found that CuO was easier to reduce than  $Cu_2O$  (Figure 3). This can be explained by the fact that the Cu(I)–O bond is much stronger than the Cu(II)–O bond (there are fewer Cu(I)–O bonds in  $Cu_2O$  than Cu(II)–O bonds in CuO). If  $Cu_2O$  is an intermediate in the CuO reduction pathway, one would always expect to see  $Cu_2O$  formation because  $Cu_2O$  would not be reduced as fast as CuO. However, if there is another  $CuO_x$  intermediate that is less stable and more reactive than  $Cu_2O$ ,<sup>23</sup>  $Cu_2O$  would not be observed. One possible intermediate is a CuO structure with 50% O vacancies that has been shown to be less stable than  $Cu_2O$ .<sup>23</sup> This species would have a diffraction pattern similar to CuO and would not appear as a separate phase.

The coexistence of phases shown in Figure 5 is consistent with a nonuniform reduction of the CuO samples. Based on this and the results of refinements, one can propose the mechanism shown in Figure 11. The initial system formed is a modified CuO that has surface sites that are efficient for the adsorption of CO ( $A \rightarrow B$ ). An induction time was always observed and became shorter at higher temperatures (Figure 3a). During this induction time, geometry relaxation could occur and surface defects could be formed. A small amount of O vacancies could be created without changing the CuO XRD pattern. Next, CuO could evolve into a nonstoichiometric metastable species ( $B \rightarrow C$ ).<sup>23</sup> This metastable species could transform to either metallic Cu directly ( $C \rightarrow H$ ), under a large supply of CO, or to a  $Cu_2O$ -like intermediate phase ( $C \rightarrow D$ ), under a low supply of CO. The  $Cu_2O$ -like phase generated is highly disordered with

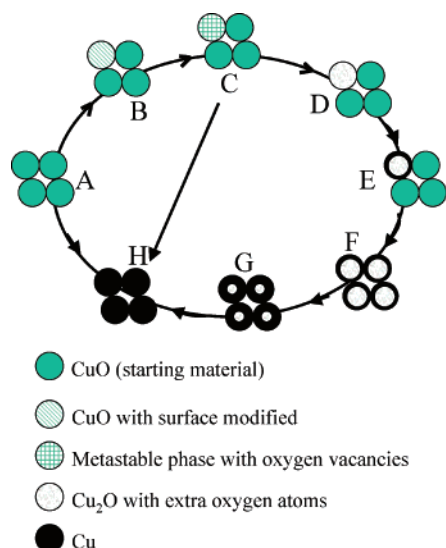


**Figure 11.** Proposed mechanism for the CuO reduction in CO gas.

a substantial amount of extra oxygen moving around the free spaces of the oxide lattice. Further reduction with CO would produce metallic copper (D  $\rightarrow$  E). The metallic copper starts to form from the surface of the Cu<sub>2</sub>O particles, and gradually becomes thicker. As the layer of Cu becomes thicker, it is more difficult to fully reduce the Cu<sub>2</sub>O (E  $\rightarrow$  F  $\rightarrow$  G). The full reduction (G  $\rightarrow$  H) would be facilitated by high temperature.

At different stages of the CuO reduction process, the rate limiting-step can be different. Initially, it is critical to generate sites for the adsorption of CO. Once a few of these sites are available, the removal of O can start (i.e., the creation of more adsorption sites for CO) and the reaction becomes autocatalytic. In the following stages, the movement of O from the bulk to the surface or the nucleation of a phase of metallic copper should become extremely important. Hence, this gas–solid reaction is typified by complex kinetics that cannot be described by a single  $n^{\text{th}}$ -order expression over the entire process. In fact, we attempted to fit different portions of the kinetic data in Figures 3 and 8 with a single  $n^{\text{th}}$  polynomial without obtaining good fittings.

## 5. Conclusion

The reactions of CuO and Cu<sub>2</sub>O with CO were investigated in detail using temperature-programmed reduction (TPR), synchrotron-based time-resolved X-ray diffraction and X-ray absorption fine structure techniques. The TPR results showed that Cu<sub>2</sub>O reduced at higher temperature than CuO did under the same operating conditions. A direct transformation pathway was observed for the isothermal reductions of both CuO and Cu<sub>2</sub>O under a large CO supply, while a step pathway with one intermediate (CuO  $\rightarrow$  Cu<sub>2</sub>O  $\rightarrow$  Cu) was seen under a limited CO supply. This was confirmed by both time-resolved X-ray diffraction and X-ray absorption fine structure techniques. The formed Cu<sub>2</sub>O was highly disordered with a substantial amount of extra oxygen embedded in the lattice. Neither Cu<sub>4</sub>O<sub>3</sub> nor an amorphous CuO<sub>x</sub> phase was formed during the reduction of CuO by CO.

This study illustrates how complex the reduction of a metal oxide by CO can be. The reduction mechanism can vary considerably with the experimental conditions (gas flow rate, temperature, sample size, etc.), and its complex kinetics cannot

be described by a single  $n^{\text{th}}$ -order expression over the entire range of reaction.

**Acknowledgment.** The research carried out at the Chemistry Department of Brookhaven National Laboratory was financed through contract DE-AC02-98CH10086 with the U.S. Department of Energy (DOE, Division of Chemical Sciences). A.I.F. acknowledges support by the U.S. Department of Energy Grant No. DE-FG02-03ER15477. The authors would like to thank Avital Merl and Pesia Soloveichik for their help in XAS data collection and processing. The National Synchrotron Light Source is supported by the Divisions of Materials and Chemical Sciences in the Office of Basic Energy Sciences at DOE.

## References and Notes

- (1) Kummer, J. T. *Prog. Energy Combust. Sci.* **1980**, *6*, 177.
- (2) Huang, T. J.; Yu, T.-C. *Appl. Catal.* **1991**, *71*, 275.
- (3) Klier, K. *Adv. Catal.* **1982**, *31*, 243.
- (4) Newsome, D. S. *Catal. Rev.* **1980**, *21* (2), 275.
- (5) PDF #41-0254, JCPDS Powder Diffraction File; Int. Center For Diffraction Data: Swarthmore, PA, 1989.
- (6) PDF #05-0667, JCPDS Powder Diffraction File; Int. Center For Diffraction Data: Swarthmore, PA, 1989.
- (7) O'Keefe, M.; Bovin, J. O. *Am. Mineral.* **1978**, *63*, 180.
- (8) PDF #083-1665, JCPDS Powder Diffraction File; Int. Center For Diffraction Data: Swarthmore, PA, 2004.
- (9) O'Keefe, M.; Moore, W. J. *J. Chem. Phys.* **1962**, *36*, 3009.
- (10) Huang, T. J.; Tsai, D.-H. *Catal. Lett.* **2003**, *87* (4), 173.
- (11) Nagase, K.; Zheng, Y.; Kodama, Y.; Kakuta, J. *J. Catal.* **1999**, *187*, 123.
- (12) Wang, J. B.; Tsai, D.-H.; Huang, T. J. *J. Catal.* **2002**, *208*, 370.
- (13) Dow, W.-P.; Huang, T. J. *J. Catal.* **1994**, *147*, 322.
- (14) (a) Martínez-Arias, A.; Fernández-García, M.; Gálvez, O.; Coronado, J. M.; Anderson, J. A.; Conesa, J. C.; Soria, J.; Munuera, G. *J. Catal.* **2000**, *195*, 207. (b) Martínez-Arias, A.; Fernández-García, M.; Hungria, A. B.; Iglesias-Juez, A.; Gálvez, O.; Anderson, J. A.; Conesa, J. C.; Soria, J.; Munuera, G. *J. Catal.* **2003**, *214*, 261.
- (15) Severino, F.; Brito, J. L.; Laine, J.; Fierro, J. L. G.; López Agudo, A. *J. Catal.* **1998**, *177*, 82.
- (16) Dow, W.-P.; Huang, T. J. *J. Catal.* **1996**, *160*, 171.
- (17) Liu, W.; Flytzani-Stephanopoulos, M. *J. Catal.* **1995**, *153*, 317.
- (18) Nakamura, J.; Campbell, J. M.; Campbell, C. T. *J. Chem. Soc., Faraday Trans.* **1990**, *86*, 2725.
- (19) Rodriguez, J. A.; Goodman, D. W. *Surf. Sci. Reports* **1991**, *14*, 1.
- (20) Li, J.-L.; Takeguchi, T.; Inui, T. *Appl. Catal. A* **1996**, *139*, 97.
- (21) Sadykov, V. A.; Tikhov, S. F. *J. Catal.* **1997**, *165*, 279.
- (22) Kung, H. H. *Transition Metal Oxides: Surface Chemistry and Catalysis*; Elsevier: New York, 1989.
- (23) Kim, J. Y.; Rodriguez, J. A.; Hanson, J. C.; Frenkel, A. I.; Lee, P. L. *J. Am. Chem. Soc.* **2003**, *125*, 10684.
- (24) Rodriguez, J. A.; Kim, J. Y.; Hanson, J. C.; Perez, M.; Frenkel, A. I. *Catal. Lett.* **2003**, *85* (3-4), 247.
- (25) Norby, P.; Hanson, J. C. *Catal. Today* **1998**, *39*, 301.
- (26) Frenkel, A.; Kleinfeld, O.; Wasserman, S. R.; Sagi, I. *J. Chem. Phys.* **2002**, *117*, 9449.
- (27) Chupas, P. J.; Ciruolo, M. F.; Hanson, J. C.; Grey, C. P. *J. Am. Chem. Soc.* **2001**, *123*, 1694.
- (28) *Gmelins Handbuch Der Anorganischen Chemie*; Kupfer Tell A, System-Nummer 60, 1955; Verlag Chemie, GmbH, Weinheim, Bergstrasse.
- (29) Hammersely, A. P.; Svensson, S. O.; Thompson, A. *Nucl. Instrum. Methods Phys. Res.* **1994**, *346*, 321.
- (30) IDL, Version 5.5; Research System, Inc., 2002.
- (31) (a) Larson, A. C.; von Dreele, R. B. *GSAS General Structure Analysis System*. Report LAUR 86-748; Los Alamos National Laboratory: Los Alamos, 1995. (b) Reitveld, A. M. *J. Appl. Cryst.* **1969**, *2*, 65.
- (32) Frenkel, A. I.; Rehr, J. J. *Phys. Rev. B* **1993**, *48*, 585.
- (33) Newville, M.; Ravel, B.; Haskel, D.; Rehr, J. J.; Stern, E. A.; Yacoby, Y.; *Physica B* **1995**, *208 & 209*, 154.
- (34) Tsai, D.-H.; Huang, T. J. *Appl. Catal. A* **2002**, *223*, 1.
- (35) Rodriguez, J. A.; Hanson, J. C.; Frenkel, A. I.; Kim, J.-Y.; Perez, M. *J. Am. Chem. Soc.* **2002**, *124*, 346.
- (36) Zuo, J. M.; Kim, M.; O'Keefe, M.; Spence, J. C. H. *Nature* **1999**, *401*, 49.